RASEI
RENEWABLE AND SUSTAINABLE ENERGY INSTITUTE

NSF International Research Experience for Students (IRES)
Perovskites – A Solution to Global Energy Conversion Needs

Computational Investigation of $MAPbI_3$ Solvent Intermediate Phases

Gabriel Graf
Department of Solution Processing of Hybrid Materials and Devices (SE-ALM)
Helmholtz-Zentrum Berlin für Materialien und Energie
Hahn-Meitner-Platz 1 14109
Berlin, Germany
gabriel.graf@duke.edu

Present address:
Thomas Lord Department of Mechanical Engineering and Materials Science
Duke University
144 Hudson Hall Campus Box 90300
Durham, NC 27708
gabriel.graf@duke.edu

Abstract
Methylammonium lead iodide ($MAPbI_3$) is a solution-processable, three-dimensional hybrid organic-inorganic perovskite (HOIP) that has served as a model structure for early research into perovskite-based photovoltaics. The performance of perovskite-based devices depends on film quality, which is governed by the chemical pathway followed during crystallization. Previous literature has revealed the formation of three possible solvent intermediate phases during the crystallization of $MAPbI_3$ from dimethylformamide (DMF) solution. The morphological differences between the solvent intermediate phases are maintained in the final perovskite film upon annealing, indicating that some solvent intermediates may be more ideal for forming high-quality perovskite films. While initial work mapping the chemical phase space of this system experimentally is underway, a theoretical treatment of the thermodynamics of this system has not yet been presented. In this report, we discuss the preparation of experimentally refined solvent intermediate crystal structures for chemical phase space mapping using density functional theory. The agreement between experimental and computationally optimized atomic positions and lattice parameters is assessed. Finally, one possible method for the quick identification of solvent intermediate phases in solution without the need for structural refinement is presented.

Introduction
One issue inhibiting the commercialization of hybrid organic-inorganic perovskite (HOIP) photovoltaics is the poor reproducibility of high power conversion efficiencies (PCEs). These PCEs are highly dependent on perovskite film quality, as in other semiconductors[1,2]. Solution-processed films should be uniformly distributed and pinhole-free for best performance. Large grain sizes are also beneficial to prevent electron impedance and charge carrier recombination at grain boundaries, although these effects are less pronounced in perovskites compared to other semiconductors[3,4]. The quality of a perovskite film depends on a large number of methodological parameters that must be controlled during synthesis. These include (anti)solvent choice, the concentration and ratio of precursors, substrate temperature, atmospheric conditions, additive choice and concentration, and annealing temperatures and times. Much attention in the perovskite community has been devoted to the optimization of these parameters using

data-driven approaches, and recently, high-throughput autonomous labs[5–8]. Despite exciting advances, a fundamental understanding of the chemical processes that lead to high-quality perovskite films is becoming increasingly necessary to sustain the continued improvements in perovskite device performance and longevity.

Multiple studies on perovskite growth have revealed a two-step crystallization pathway, involving the formation of a solvent intermediate phase[9–11]. The solvent intermediate phase is then transformed into the final perovskite film upon annealing. Importantly, the morphology of the intermediate phase is often maintained in the final perovskite film[9,12]. The compositional and morphological differences of these phases indicate that some intermediates may be more ideal for producing high-quality perovskite films than others. It is therefore crucial to identify which phases are desirable and understand the mechanisms associated with their formation.

In 2017, Petrov *et al.* refined the crystal structures of three solvent intermediate phases from $MAPbI_3$ crystallization in a dimethylformamide (DMF) solution using X-ray diffraction (XRD) data (shown in **Figure 1**)[9]. They recognized that the selective formation of a solvent intermediate phase depended heavily on the PbI_2:MAI ratio in the solution. They also found that the morphologies of the intermediate phases were maintained in the final perovskite upon annealing. Since then, they have also made progress in mapping the chemical phase space of this system experimentally[13]. The availability of crystal structures from XRD opens the door for an atomistic, first-principles computational investigation into the properties of these intermediates. This can provide insight into the thermodynamic nature of these phases, allow for finer control over the crystallization, and enhance the reproducibility of high-quality perovskite films. In this report, we discuss the preparation of the experimental structures from Petrov *et al.* for first-principles thermodynamics calculations using density functional theory (DFT). We also describe a method for the quick identification of these solvent intermediate states from experimental XRD patterns.

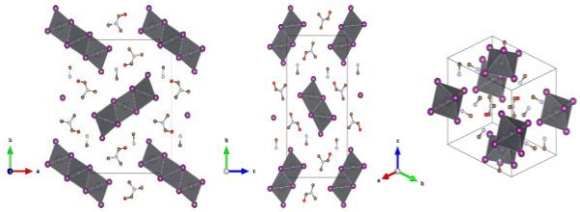

Figure 1. Three crystal structures of $MAPbI_3$ solvent intermediates from Petrov et al. 2017[9].

It is well-known that hydrogen atoms are systematically misplaced in XRD structures due to their poor X-ray scattering ability[14]. This frequently leads to incorrect bond lengths and directions in experimental XRD structures. We have applied the technique introduced by Xie *et al.* to correct the hydrogen positions in these structures[14]. This first involves constraining the lattice vector lengths and angles, as well as the positions of all non-hydrogen atoms to their experimentally determined values. The hydrogen atom positions are then computationally relaxed to their most energetically favorable positions using DFT. This method has been shown to produce structures that are in excellent agreement with neutron scattering results[14]. Additionally, we conduct a full relaxation of the lattice parameters and atomic positions to determine the nearest energetic minimum for each structure, as determined by DFT. Finally, we conducted a relaxation of the organic and solvent molecules, while holding the cell parameters and inorganic ions fixed. This was done to test the validity of the experimentally refined organic molecule positions and orientations. The all-electron, scalable electronic structure theory package FHI-aims was used with "intermediate" default basis sets for all DFT calculations in this study. All structures were calculated at the Perdew-Burke-Ernzerhof (PBE) level of theory, with the Tkatchenko-Scheffler (TS) van der Waals (vdW) correction to capture long-range electrostatic interactions[15]. The Broyden-Fletcher-Goldfarb-Shanno (BFGS) algorithm was used for numerical geometry optimization, with a maximum residual force per atom of 0.005 eV/Å.

Results & Discussion

The average position change for each species during the hydrogen-only and organic-only relaxations, as well as the lattice parameter changes for the full relaxation, are

given in **Table 1** and **Table 2**. The hydrogen displacements during the hydrogen-only relaxation are on the same scale as those reported in other HOIP systems[14]. Furthermore, minimal atomic displacements are observed from the experimental structure when the organic molecules (DMF and MA^+) are relaxed. This indicates that the refined atomic positions of carbon, nitrogen, and oxygen are close to a minimum on the theoretical potential energy surface when other positions and parameters are taken as fixed. The full DFT relaxations also show good agreement with the experimentally refined crystal structures. Two interesting observations appear within this data: the consistently smaller volume of the DFT-relaxed cell and the deviation of the α angle from 90° in fully-relaxed $(MA)_2(DMF)_2Pb_3I_8$. Both of these observations can be explained by the inherent lack of finite temperature effects in standard DFT calculations. Thermal expansion of the unit cell contributes to the larger volume measured at finite temperature (100K) during the experiment. Likewise, temperature increases are known to lead to the formation of higher symmetry systems. This is readily apparent in 3D perovskite systems such as $MAPbI_3$, where three distinct phase transitions occur from a lower symmetric phase to higher symmetric phase with increasing temperature[16].

Table 1. Average displacement of each species in the DFT-relaxed structures from the experimentally reported XRD structure in the hydrogen-only and organics-only relaxations. Lead and iodide displacements are not shown as these atoms were constrained in both relaxations.

Intermediate Phase	Species	Hydrogen-only Displacements (Å)	Organics-only Displacements (Å)
$(MA)_2(DMF)_2Pb_3I_8$	H	**0.13 ± 0.02**	**0.14 ± 0.06**
	C	0.00 ± 0.00	**0.05 ± 0.03**
	N	0.00 ± 0.00	**0.08 ± 0.05**
	O	0.00 ± 0.00	**0.04 ± 0.00**
$(MA)_2(DMF)_2Pb_2I_6$	H	**0.14 ± 0.02**	**0.15 ± 0.05**
	C	0.00 ± 0.00	**0.08 ± 0.03**
	N	0.00 ± 0.00	**0.07 ± 0.01**
	O	0.00 ± 0.00	**0.11 ± 0.00**
$(MA)_3(DMF)PbI_5$	H	**0.16 ± 0.05**	**0.17 ± 0.05**
	C	0.00 ± 0.00	**0.07 ± 0.02**
	N	0.00 ± 0.00	**0.08 ± 0.02**
	O	0.00 ± 0.00	**0.11 ± 0.00**

Table 2. Unit cell lattice parameters for experimental and fully relaxed DFT structures.

Intermediate Phase	Exp/ DFT	Lengths (Å)			Angles (°)			Volume (Å³)
		a	b	c	α	β	γ	
$(MA)_2(DMF)_2Pb_3I_8$	Exp	17.2	22.0	4.6	90.	90.	90.	1717
	DFT	17.4	21.8	4.5	88	90.	90.	1714
$(MA)_2(DMF)_2Pb_2I_6$	Exp	4.6	25.5	12.1	90.	97	90.	1398
	DFT	4.5	25.5	12.1	90.	96	90.	1387
$(MA)_3(DMF)PbI_5$	Exp	10.2	11.4	12.4	111	101	110.	1170.
	DFT	10.2	11.3	12.4	111	101	111	1153

Using the crystallographic visualization software VESTA, we have additionally plotted the simulated powder XRD patterns of each computationally relaxed structure for every intermediate. This allows us to compare how minor displacements within the structure from computational relaxation affect the simulated XRD pattern. Furthermore, by identifying peaks that remain unchanged, we can identify regions that could be useful for quick identification of solvent intermediate phases without the need for structural refinement. These spectra are shown in **Figures 3a-c.** From analysis of these simulated spectra, it is apparent that hydrogen positions play a definite role in peak intensity. Furthermore, lateral peak shifts appear in the fully-relaxed structures. Critically, these spectra can also be divided into two regions. First is a region from $0 < 2\theta < 20°$, which does not appear to change noticeably with minor deviations in lattice parameters or atomic positions. Second is a region $20° < 2\theta$, which could be thought of as a "fingerprint" region, in which any minor deviations can significantly affect the spectrum. It is also worth noting that the spectra for each intermediate phase are noticeably different from each other in the first region. This, combined with the relative invariance of the peaks to minor deviations, suggests that this could be a highly useful region for the quick identification of which intermediate is formed under any given conditions.

a.

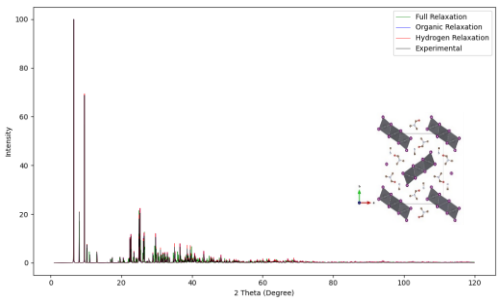

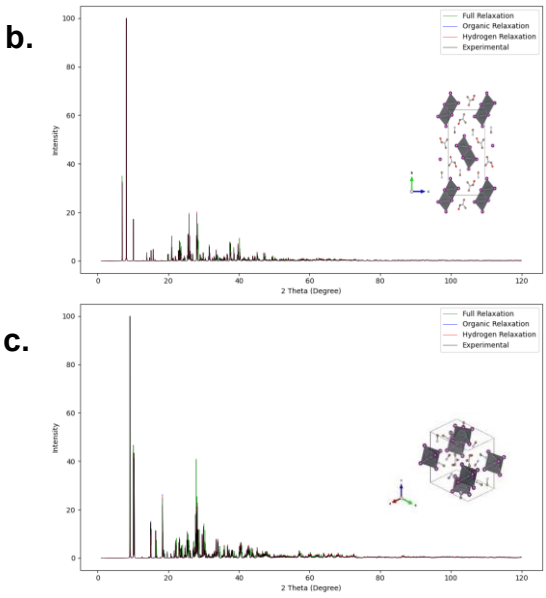

Figure 3a-c. Simulated powder XRD patterns for each relaxed structure of (a) $(MA)_2(DMF)_2Pb_3I_8$, (b) $(MA)_2(DMF)_2Pb_2I_6$, and (c) $(MA)_3(DMF)PbI_5$.

Conclusions

When fully relaxed using DFT, all three solvent intermediate phases show similar lattice parameters to the experimentally refined crystal structures. This indicates that the experimental solvent intermediate structures are near a minimum on the potential energy surface and stable according to theory. The hydrogen atoms show systematic misplacements typical in experimental XRD structures, which were corrected using hydrogen-only DFT relaxation. Relaxing the organic molecules yielded only minimal changes in the structure, indicating that their components have been adequately refined in the XRD structure. These structures can now serve as a basis for further calculations to study the thermodynamic phase space of this system. Finally, we propose that the $0 < 2\theta < 20°$ range of the XRD spectrum can be used for the quick identification of solvent intermediate phases during the two-step crystallization of $MAPbI_3$ from DMF solution.

Acknowledgements

This work is primarily supported by the National Science Foundation (NSF) IRES: US - Germany: Perovskites - A Solution to Global Energy Conversion Needs (Award No. 2419757). I would like to thank Professor Eva Unger for hosting me in the SE-ALM group at Helmholtz-Zentrum Berlin and for many insightful discussions related to my project's motivation and execution. I would like to thank my graduate student research mentor, Anton Dzhong, for providing me with the resources and experimental perspective necessary to make progress on my project. I would also like to thank Professor Volker Blum at Duke University for his continued support of my project from my initial application to the program through its current state, as well as for his guidance on the theoretical and computational techniques required to complete this project. Finally, I would like to thank Dr. Lauren Scholz at the University of Colorado Boulder for organizing and coordinating this entire exchange program and ensuring that all the exchange students had access to the resources they needed and an enjoyable and productive stay.

References

(1) Meillaud, F.; Boccard, M.; Bugnon, G.; Despeisse, M.; Hänni, S.; Haug, F.-J.; Persoz, J.; Schüttauf, J.-W.; Stuckelberger, M.; Ballif, C. Recent Advances and Remaining Challenges in Thin-Film Silicon Photovoltaic Technology. *Materials Today* **2015**, *18* (7), 378–384. https://doi.org/10.1016/j.mattod.2015.03.002.

(2) Huang, J.; Gao, C.; Zhang, D.; Tian, Q.; Zhang, F.; Liu, S. (Frank). Influence of Film Quality on Power Conversion Efficiency in Perovskite Solar Cells. *Coatings* **2019**, *9* (10), 622. https://doi.org/10.3390/coatings9100622.

(3) Yin, W.-J.; Yang, J.-H.; Kang, J.; Yan, Y.; Wei, S.-H. Halide Perovskite Materials for Solar Cells: A Theoretical Review. *J. Mater. Chem. A* **2015**, *3* (17), 8926–8942. https://doi.org/10.1039/C4TA05033A.

(4) Sherkar, T. S.; Momblona, C.; Gil-Escrig, L.; Ávila, J.; Sessolo, M.; Bolink, H. J.; Koster, L. J. A. Recombination in Perovskite Solar Cells: Significance of Grain Boundaries, Interface Traps, and Defect Ions. *ACS Energy Lett.* **2017**, *2* (5), 1214–1222. https://doi.org/10.1021/acsenergylett.7b00236.

(5) Miftahullatif, E. B.; Pethe, S. D.; Low, A. K. Y.; Zhumekenov, A. A.; Yantara, N.; Kajal, P.; Wu, Q.; Jie Tay, D. J.; Sharma, D.; Sebastian, S.; Recatala-Gomez, J.; Abhishek, N.; Mathews, N.;

Hippalgaonkar, K. Machine-Learning-Driven in-Device Optimization of All-Printed Perovskite Solar Cells. *ACS Energy Lett.* **2025**, 3952–3961. https://doi.org/10.1021/acsenergylett.5c01475.

(6) Zhang, J.; Liu, B.; Liu, Z.; Wu, J.; Arnold, S.; Shi, H.; Osterrieder, T.; Hauch, J. A.; Wu, Z.; Luo, J.; Wagner, J.; Berger, C. G.; Stubhan, T.; Schmitt, F.; Zhang, K.; Sytnyk, M.; Heumueller, T.; Sutter-Fella, C. M.; Peters, I. M.; Zhao, Y.; Brabec, C. J. Optimizing Perovskite Thin-Film Parameter Spaces with Machine Learning-Guided Robotic Platform for High-Performance Perovskite Solar Cells. *Advanced Energy Materials* **2023**, *13* (48), 2302594. https://doi.org/10.1002/aenm.202302594.

(7) Ahmadi, M.; Ziatdinov, M.; Zhou, Y.; Lass, E. A.; Kalinin, S. V. Machine Learning for High-Throughput Experimental Exploration of Metal Halide Perovskites. *Joule* **2021**, *5* (11), 2797–2822. https://doi.org/10.1016/j.joule.2021.10.001.

(8) Kirman, J.; Johnston, A.; Kuntz, D. A.; Askerka, M.; Gao, Y.; Todorović, P.; Ma, D.; Privé, G. G.; Sargent, E. H. Machine-Learning-Accelerated Perovskite Crystallization. *Matter* **2020**, *2* (4), 938–947. https://doi.org/10.1016/j.matt.2020.02.012.

(9) Petrov, A. A.; Sokolova, I. P.; Belich, N. A.; Peters, G. S.; Dorovatovskii, P. V.; Zubavichus, Y. V.; Khrustalev, V. N.; Petrov, A. V.; Grätzel, M.; Goodilin, E. A.; Tarasov, A. B. Crystal Structure of DMF-Intermediate Phases Uncovers the Link Between CH3NH3PbI3 Morphology and Precursor Stoichiometry. *J. Phys. Chem. C* **2017**, *121* (38), 20739–20743. https://doi.org/10.1021/acs.jpcc.7b08468.

(10) Xiang, W.; Zhang, J.; Liu, S. (Frank); Albrecht, S.; Hagfeldt, A.; Wang, Z. Intermediate Phase Engineering of Halide Perovskites for Photovoltaics. *Joule* **2022**, *6* (2), 315–339. https://doi.org/10.1016/j.joule.2021.11.013.

(11) Li, Y.; Zhi, L.; Ge, G.; Zhao, Z.; Cao, X.; Chen, F.; Cui, X.; Lin, F.; Ci, L.; Sun, J.; Zhuang, D.; Wei, J. Investigation on Crystallization of $CH_3NH_3PbI_3$ Perovskite and Its Intermediate Phase from Polar Aprotic Solvents. *Crystal Growth & Design* **2019**, *19* (2), 959–965. https://doi.org/10.1021/acs.cgd.8b01516.

(12) Zhang, K.; Zhao, Y.; Duan, R.; Huang, P.; Zhu, K.; Li, Z.; Dong, B.; Zhou, Y.; Zhu, H.; Song, B. Improve the Crystallinity and Morphology of Perovskite Films by Suppressing the Formation of Intermediate Phase of CH3NH3PbCl3. *Organic Electronics* **2019**, *68*, 96–102. https://doi.org/10.1016/j.orgel.2019.01.044.

(13) Petrov, A. A.; Ordinartsev, A. A.; Lyssenko, K. A.; Goodilin, E. A.; Tarasov, A. B. Ternary Phase Diagrams of MAI–PbI_2–DMF and MAI–PbI_2–DMSO Systems. *J. Phys. Chem. C* **2022**, *126* (1), 169–173. https://doi.org/10.1021/acs.jpcc.1c10062.

(14) Xie, Y.; Koknat, G.; Weadock, N. J.; Wang, X.; Song, R.; Toney, M. F.; Blum, V.; Mitzi, D. B. Hydrogen Bonding Analysis of Structural Transition-Induced Symmetry Breaking and Spin Splitting in a Hybrid Perovskite Employing a Synergistic Diffraction-DFT Approach. *J. Am. Chem. Soc.* **2024**, *146* (32), 22509–22521. https://doi.org/10.1021/jacs.4c06287.

(15) Tkatchenko, A.; Scheffler, M. Accurate Molecular Van Der Waals Interactions from Ground-State Electron Density and Free-Atom Reference Data. *Phys. Rev. Lett.* **2009**, *102* (7), 073005. https://doi.org/10.1103/PhysRevLett.102.073005.

(16) Whitfield, P. S.; Herron, N.; Guise, W. E.; Page, K.; Cheng, Y. Q.; Milas, I.; Crawford, M. K. Structures, Phase Transitions and Tricritical Behavior of the Hybrid Perovskite Methyl Ammonium Lead Iodide. *Sci Rep* **2016**, *6* (1), 35685. https://doi.org/10.1038/srep35685.